International Journal of Nanomedicine

Dovepress

open access to scientific and medical research

Open Access Full Text Article

ORIGINAL RESEARCH

Combined Self-Assembled Hendeca-Arginine Nanocarriers for Effective Targeted Gene Delivery to Bladder Cancer

Pu Zhang[1,*], Haibao Zhang[2,*], Bin Zheng[1,*], Heng Wang[1], Xiaolong Qi[1], Shuai Wang[1], Zhenghong Liu[1], Li Sun[1], Yang Liu[3], Xiaowen Qin[1], Weijiao Fan[1], Minghai Ma[2], Wing-Fu Lai[1], Dahong Zhang[1]

[1]Urology & Nephrology Center, Department of Urology, Zhejiang Provincial People's Hospital, Affiliated People's Hospital, Hangzhou Medical College, Hangzhou, Zhejiang People's Republic of China; [2]Key Laboratory of Environment and Genes Related to Diseases, Xi'an Jiaotong University, Xi'an, People's Republic of China; [3]Cancer Center, Department of Ultrasound Medicine, Zhejiang Provincial People's Hospital, Affiliated People's Hospital, Hangzhou Medical College, Hangzhou, Zhejiang People's Republic of China

*These authors contributed equally to this work

Correspondence: Dahong Zhang; Wing-Fu Lai, No. 138 Shang Tang Road, Hangzhou, 310014, People's Republic of China, Tel +86-13705711671, Email zppurology@163.com; rori0610@graduate.hku.hk

Introduction: Bladder cancer (BCa) is among the most prevalent cancers worldwide. However, the effectiveness of intravesical therapy for BCa is limited due to the short dwell time and the presence of the permeation barrier.

Methods: Nanocomplexes were self-assembled between DNA and hendeca-arginine peptide (R11). Stepwise intravesical instillation of R11 and the generated nanocomplexes significantly enhanced the targeting capacity and penetration efficiency in BCa therapy. The involved mechanism of cellular uptake and penetration of the nanocomplexes was determined. The therapeutic effect of the nanocomplexes was verified preclinically in murine orthotopic BCa models.

Results: Nanocomplexes exhibited the best BCa targeting efficiency at a nitrogen-to-phosphate (NP) ratio of 5 but showed a lack of stability during cellular uptake. The method of stepwise intravesical instillation not only increased the stability and target specificity of the DNA component but also caused the delivered DNA to more effectively penetrate into the glycosaminoglycan layer and plasma membrane. The method promotes the accumulation of the delivered DNA in the clathrin-independent endocytosis pathway, directs the intracellular trafficking of the delivered DNA to nonlysosome-localized regions, and enables the intercellular transport of the delivered DNA via a direct transfer mechanism. In preclinical trials, our stepwise method was shown to remarkably enhance the targeting and penetration efficiency of DNA in murine orthotopic BCa models.

Conclusion: With this method, a stepwise intravesical instillation of self-assembled nanocomplexes, which are generated from hendeca-arginine peptides, was achieved; thus, this method offers an effective strategy to deliver DNA to target and penetrate BCa cells during gene therapy and warrants further development for future intravesical gene therapy in the clinical context.

Keywords: bladder cancer, intravesical therapy, DNA delivery, direct transfer

Introduction

Bladder cancer (BCa) is among the most prevalent cancers worldwide. Approximately 550,000 individuals are diagnosed with BCa annually, and almost 40% of patients succumb to the disease.[1] For patients who are initially diagnosed with non-muscle-invasive BCa, transurethral resection of the bladder tumor followed by intravesical therapy (IT) is often performed.[2] IT is used to kill the residual tumor and prevent recurrence and progression. However, the effectiveness of IT is limited.[3] Constant cycling of urine and normal voiding reduces the exposure time and the concentration of drugs to BCa. Additionally, BCa tissue is composed of densely packed cellular aggregates and paracellular matrix. Together with the protective glycosaminoglycan (GAG) layer, BCa tissue serves as an obstacle to drug penetration during IT.[3] To improve the dwell-time of IT drugs in BCa tissue, intravesical gene-based drugs, which have long-term effects on their

Received: 1 July 2022
Accepted: 6 September 2022
Published: 22 September 2022

Graphical Abstract

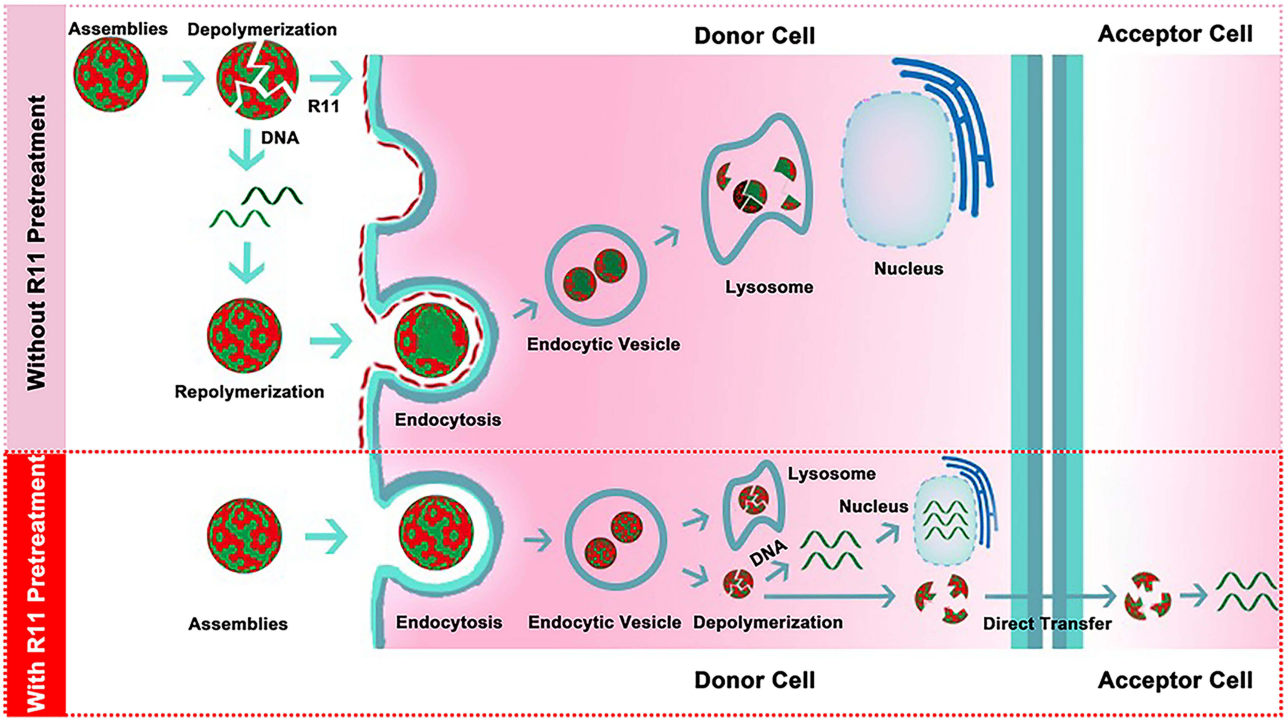

targets, have been extensively developed and applied preclinically.[3] Intravesical gene-based drugs are mostly loaded into viral vectors or cationic liposomes for gene therapy.[4] However, drugs that exhibit poor BCa specificity produce adverse effects on the normal urothelium.[4] Their penetration efficacies also remain far from satisfactory owing to their reliance on passive penetration.[5] These drawbacks drive the need to develop alternative carriers for gene therapy to address BCa.

Over the years, different types of carriers other than viral vectors and liposomes have been proposed for BCa gene therapy, ranging from inorganic nanoparticles[6,7] to polymers.[8] Among them, polymers with a proteinaceous nature have attracted extensive interest because of their target specificity and structural flexibility. Previously, we adopted the hendeca-arginine peptide (R11) to generate nanoprobes to perform molecular imaging of spherical nucleic acids, leading to effective identification of bladder cancer margins and a significant improvement in the R0 resection rate in surgery.[9] We also observed that R11 peptides have the potential to significantly increase the BCa targeting ability and membrane penetrability of nucleic acid materials during bioimaging.[9] Because R11 is positively charged, it can interact with the negatively charged phosphate backbone of nucleic acids (including RNA and DNA) through electrostatic interactions to self-assemble into nanocomplexes.[10] This makes R11 a potential carrier for cancer gene therapy. Despite such potential, in the case of BCa treatment, nanocomplexes that form from R11 are easily depolymerized when they contact negatively charged components in the GAG layer and the BCa tissue, severely retarding the practical potential of R11 in the mediation of gene therapy for BCa. This study addressed this problem by utilizing the method of stepwise intravesical instillation and successfully preserved the stability of the nanocomplexes to effectively deliver DNA across the GAG layer and the plasma membrane with high specificity. Our stepwise method can also direct the intracellular trafficking of the delivered DNA toward nonlysosome-localized regions and can boost the intercellular trafficking of the DNA component through the direct transfer mechanism. The effectiveness of this stepwise method was further verified preclinically in murine orthotopic BCa models. Along with the simplicity of synthesis, the stepwise method offers translational advantages and warrants further development as a therapeutically potent strategy for gene-based IT.

Materials and Methods

Preparation of R11-DNA Nanocomplexes at Different NP Ratios

Solutions that contained nanocomplexes were prepared by mixing one volume of an R11 solution to an equal volume of a DNA solution at different ratios of the total nitrogen number from R11 to the phosphate number from DNA (NP ratios). The NP ratios for each type of R11-DNA nanocomplex were set as 5, 10 and 20. The generated nanocomplexes were designated NP5, NP10, and NP20. During nanocomplex preparation, the DNA solution was added dropwise into the R11 solution under vigorous stirring as previously described.[11]

Determination of the Physicochemical Properties of R11-DNA Nanocomplexes at Different NP Ratios

The physicochemical properties of R11-DNA nanocomplexes at different NP ratios included the size distribution, zeta potential, morphology, migration efficiency in gel and fluorescence emission spectrum. The size distribution and zeta potential of the nanocomplexes, which contained an R11 concentration of 2 μM, were analyzed by using a Zetasizer (Malvern Zetasizer; Malvern Ins. Ltd., Malvern, UK) at 25 °C in PBS buffer. To perform the gel retardation assay, nanocomplexes, which contained a DNA concentration of 0.5 μM, were loaded into a 2% (w/v) agarose gel stained with Gel Red (APExBIO Technology, Houston, US). Electrophoresis was carried out at 100 V in TAE buffer for 40 min. DNA bands were visualized under a transilluminator. All scanning electron microscopy (SEM) images were obtained using SEM (Model S4800; Hitachi Ltd., Tokyo, Japan) after the nanocomplexes were simply deposited on freshly cleaved silicon wafers and dried in air. The fluorescence spectrum of the nanocomplexes was determined using a Multi-Mode Microplate Reader (Synergy Mx, Bio-Tek Instruments Inc., Winooski, US). For the TAMRA-labeled R11, the emission spectra were measured from 572 nm to 620 nm at an excitation wavelength of 560 nm. For the FITC-labelled DNA, the emission spectra were measured from 517 nm to 560 nm at an excitation wavelength of 494 nm.

Cell Culture

SVHUC-1, T24, and 253J cells were obtained from the National Collection of Authenticated Cell Cultures, China, and were cultured in DMEM. All cell lines were supplemented with 10% fetal bovine serum and 100 U/mL 1% penicillin/streptomycin and maintained at 37 °C in a 100% humidified atmosphere containing 5% CO_2 at 37 °C. In the following experiments, T24 and 253J were used as BCa cell lines, whereas SVHUC-1 represented normal urothelial cells.

Determining the Cytotoxicity of the Nanocomplexes

A cytotoxicity assay of R11-DNA nanocomplexes at different NP ratios was performed in T24 cells. T24 cells were plated into 96-well plates (4000 cells per well) and incubated for 24 h. The cells were incubated with either nanocomplexes or free R11 for 24 h. After that, the medium in each well was replaced with 0.2 mL of fresh medium containing a 10% CCK-8 solution (Yeasen Biotechnology Co., Ltd., Shanghai, China) for another 2 h. The absorbance in each well was measured at 450 nm using a microplate spectrophotometer. Each data point was tested in triplicate in three independent experiments.

Evaluation of the BCa Specificity, Cellular Uptake Efficiency, Cellular Uptake Mechanisms and Intercellular Direct Transfer Efficiency of the Nanocomplexes

The BCa specificity, cellular uptake efficiency, cellular uptake mechanisms and intercellular direct transfer efficiency of the nanocomplexes were tested by flow cytometry. The basic flow cytometry procedure was performed as follows. Cells were grown in a 12-well plate at a density of 1×10^5 cells per well for 12 h and then incubated with fluorescent-labeled materials at designated concentrations. At regular time intervals, the cells were washed twice with PBS and digested by trypsin. Trypsinized cells were then centrifuged at 1000 rpm for 3 min to remove trypsin. The collected cells were resuspended in 1.0 mL PBS and analyzed by flow cytometry (BD Biosciences, New Jersey, US). Every 10,000 cells were counted to determine the average fluorescence intensity. The experiment was repeated three times independently. FlowJo software was used for data analyses. Data are presented as the mean±S.D.

The BCa specificity and the cellular uptake efficiency of both R11 and DNA components in nanocomplexes were tested as follows. To quantify the R11 specificity, either nanocomplexes (with the concentration of TAMRA-labeled R11 being 2.0 μM) or free TAMRA-labeled R11 (2.0 μM) were hybridized with SVHUC-1, T24 or 253J for 6 h. The average intensity was measured at the FL2 channel. To quantify the DNA specificity, nanocomplexes with a concentration of FITC-labeled DNA of 0.5 μM were hybridized with SVHUC-1, T24 or 253J for 6 h. The average intensity was measured at the FL1 channel. To quantify the internalized amount of DNA after R11 pretreatment, T24 cells were initially pretreated with 0 μM, 0.1 μM, 0.25 μM or 0.5 μM R11 for 1 h. After that, NP5 nanocomplexes with a concentration of FITC-labeled DNA of 0.5 μM were incubated with T24 for 6 h. In addition, SVHUC-1 cells were pretreated with 0 μM or 0.25 μM R11 for 1 h. NP5 nanocomplexes with a concentration of FITC-labeled DNA of 0.5 μM were then incubated with SVHUC-1 for 6 h. The average intensity was measured in the FL1 channel. NP5 nanocomplexes with a concentration of FITC-labeled DNA of 0.5 μM were incubated with pretreated T24 (in which the cells were pretreated with R11 at a concentration of 0.25 μM for 6 h before the experiment) for 6 h. The nanocomplexes were also added to T24 in the presence of R11 at a concentration of 0.25 μM for 6-h coincubation. NP5 nanocomplexes with a FITC-labeled DNA concentration of 0.5 μM were incubated with SVHUC-1 and pretreated with SVHUC-1 (in which the cells were pretreated with R11 at a concentration of 0.25 μM for 6 h before the experiment) for 6 hr. The nanocomplexes were also added to SVHUC-1 in the presence of R11 at a concentration of 0.25 μM for 6 h of coincubation. The average intensity was measured at the FL1 channel.

The cellular uptake mechanisms were explored as follows. Endocytosis inhibitors, including filipin (1.0 μg/mL), CPZ (10.0 μg/mL) or EIPA (10.0 μg/mL),[12] were separately incubated with T24 or R11-pretreated T24 cells for 1 h. NP5 nanocomplexes, either with a 2.0 μM concentration of TAMRA-labeled R11 or with a 0.5 μM concentration of FITC-labeled DNA, were separately incubated with T24 or R11-pretreated T24 cells for 2 h. NP5 nanocomplexes, either with a 2.0 μM concentration of TAMRA-labeled R11 or with a 0.5 μM concentration of FITC-labeled DNA, were separately incubated with T24 or R11-pretreated T24 at 4 °C to block energy-dependent endocytosis. The average intensity was measured at the FL1 channel for DNA or at the FL2 channel for R11.

To quantify the intercellular direct transfer efficiency of R11, T24 cells were pretreated with either 2.0 μM free Cy5-labeled R11 or nanocomplexes with a concentration of Cy5-labeled R11 of 2.0 μM for 6 h. After treatment with mitomycin C (5 μg/mL) for 3 h, R11-labeled T24 and GFP-transfected T24 cells were mixed together and cocultured in the same dish for 12 h. The cells were trypsinized to form cell suspensions for analysis. The average intensity was measured at the FL1 channel and the FL6 channel. To quantify the intercellular direct transfer efficiency of DNA, either T24 or pretreated T24 (in which the cells were pretreated with R11 at a concentration of 0.25 μM for 6 h before the experiment) was treated with nanocomplexes with 0.5 μM Cy5-labeled DNA for 6 h. After treatment with mitomycin C (5 μg/mL) for 3 h, R11-labeled T24 and GFP-transfected T24 cells were mixed together and cocultured in the same dish overnight. The cells were trypsinized to form cell suspensions for analysis. The average intensity was measured at the FL1 channel and the FL6 channel.

Evaluating the Permeation Efficiency of the Nanocomplexes

The permeation efficiency of nanocomplexes in the GAG layer or in the extracellular matrix was determined via a diffusion chamber system (Transwell diffusion chamber apparatus). In the GAG permeation assay, chondroitin sulfate (at 0.75 mg/cm^2, with or without being premixed with 0.25 μM R11) was added to the upper Transwell chamber with a 0.4 μm pore polyester membrane insert (Corning, Thermo Fisher Scientific Inc, Waltham, US). Then, 100 μL of NP5 nanocomplexes with a concentration of FITC-labeled DNA of 0.5 μM was gently added into the upper chamber, and 1 mL of PBS buffer was added into the lower chamber. The fluorescence intensity of the buffer in the lower chamber was quantified using an excitation wavelength of 494 nm and an emission wavelength of 522 nm. The concentration was calculated according to the standard curve.

In the Matrigel permeation assay, 50 μL of Matrigel was added to the upper chamber of the Transwell with a 0.4 μm pore polyester membrane insert. Then, 100 μL of either NP5 nanocomplexes (with the concentration of TAMRA-labeled R11 being 2.0 μM) or TAMRA-labeled R11 (2.0 μM) was gently added into the upper chamber. Then, 1 mL of PBS buffer was added to the lower chamber. The fluorescence intensity of the buffer in the lower chamber was quantified using an excitation wavelength of 560 nm and an emission wavelength of 583 nm. The concentration was calculated according to the standard curve. One hundred microliters of either NP5 nanocomplexes (with a concentration of FITC-labeled DNA of 0.5 μM) or

FITC-labeled DNA (0.5 μM) was gently added to the upper chamber. Then, 1 mL of PBS buffer was added to the lower chamber. The fluorescence intensity of the buffer in the lower chamber was quantified using an excitation wavelength of 494 nm and an emission wavelength of 522 nm. The concentration was calculated according to the standard curve.

Confocal Laser Scanning Microscopy (CLSM) Examination of the Subcellular Distribution of Nanocomplexes

A CLSM examination was conducted as follows. Cells were grown in a confocal dish (Solarbio Life Science Co., Ltd, Beijing, China) at a density of 1×10^5 cells per well for 12 h and then incubated with fluorescent-labeled materials at designated concentrations. At regular time intervals, the cells were washed twice with PBS and stained with dyes. The cells were washed twice with PBS before being imaged by CLSM (Leika TCS SP5 Confocal, LEIKA Inc, California, US).

To analyze the colocalization of both R11 and DNA components in nanocomplexes at the plasma membrane or in the cytoplasm, NP5 nanocomplexes (which were composed of TAMRA-labeled R11 and FITC-labeled DNA, in which the R11 concentration was 2.0 μM) were incubated with T24 or pretreated T24 (in which the cells were pretreated with R11 at a concentration of 0.25 μM for 6 h before the experiment). The excitation wavelength used was 494 nm for FITC-labeled DNA and 560 nm for TAMRA-labeled R11. ImageJ software was used for analysis.

To determine the subcellular distribution of DNA, NP5 nanocomplexes (with a 0.5 μM concentration of Cy5-labeled DNA) were incubated with T24 or pretreated T24 (in which the cells were pretreated with R11 at a concentration of 0.25 μM for 6 h before the experiment) for 6 h. The lysosomes were stained with LysoTracker green (0.2 μM). The nuclei were stained with Hoechst 33,342 (2.0 μM). The excitation wavelengths used were 405 nm for Hoechst 33,342, 488 nm for LysoTracker green, and 647 nm for Cy5-labeled DNA. ImageJ software was used for analysis.

To quantify the transcytosis efficiency of fluorescent-labeled materials, the first generation T24 cells or pretreated T24 cells (in which the cells were pretreated with R11 at a concentration of 0.25 μM for 6 h before the experiment) was incubated with either NP5 nanocomplexes (with either the concentration of Cy5-labeled DNA being 0.5 μM, or the concentration of Cy5-labeled R11 being 2.0 μM) or free Cy5-labeled R11 (2.0 μM) for 6 h. The medium containing fluorescent-labeled materials was discarded and the first generation T24 was incubated with fresh medium for 12 h. The medium containing exocytosis secretion from the first generation T24 cells was harvested, centrifuged by 5000 rpm to remove the cell debris, and incubated with the next generation T24 cells for another 12 h. The medium containing secreted products from the first generation T24 cells was discarded and the second generation T24 cells was incubated with fresh medium for 12 h. The medium containing secreted products from the second generation T24 cells was harvested, centrifuged by 5000 rpm to remove the cell debris, and incubated with the third generation T24 cells for another 12 h. The nuclei were stained with Hoechst 33,342 (2.0 μM). The excitation wavelength used was 405 nm for Hoechst 33,342 and 647 nm for Cy5-labeled DNA or Cy5-labeled R11. ImageJ software was used for analysis.

Evaluation of the Penetration Capacity of the Nanocomplexes in Multicellular Spheroids (MCSs)

To generate MCSs, T24 cells were suspended in fresh DMEM (containing 0.12% w/v methylcellulose) at a density of 1×10^6 cells per mL. A total of 25 μL of the cell suspension was dropped on the lid of the cell culture plate to form uniform droplets. Ten milliliters of PBS was added to the plate to keep the droplets moist. After 72 h, dense spheroids were transferred to a low adhesion 96-well plate with one spheroid per well and incubated for another 72 h.

A assay for the penetration of nanocomplexes in MCSs was performed as follows. To inhibit endocytosis, a cocktail containing filipin (1.0 μg/mL), CPZ (10.0 μg/mL) and EIPA (10.0 μg/mL) was used. To inhibit exocytosis, EXO1 (50 μM) was used.[13] T24 MCSs were incubated with either NP5 nanocomplexes (which were composed of TAMRA-labeled R11 and FITC-labeled DNA, with a 2.0 μM concentration of R11) or free TAMRA-labeled R11 (2.0 μM) for 6 h. T24 MCSs were washed twice with PBS and imaged by CLSM. The excitation wavelength used was 494 nm for FITC-labeled DNA and 560 nm for TAMRA-labeled R11. ImageJ software was used for analysis.

Intravesical Instillation of the Nanocomplexes in Murine Orthotopic BCa Models

All animal procedures were approved by the Laboratory Animal Management Committee at Zhejiang Provincial People's Hospital (SYXK(Zhe) 2019–0013). All animal procedures were performed according to the guidelines of the Administration Committee of Experimental Animals in Zhejiang Province and the Ethics Committee of Zhejiang Provincial People's Hospital. Six- to 8-wk-old nu/nu female mice were anesthetized by inhalation of 1% isoflurane (RWD Life Science Co., Ltd, Shenzhen, China) in an oxygen gas mixture and were placed on a heated platform during the catheterization procedures. Lubricated angiocatheters were inserted into the urethra. After full insertion, the bladder was flushed with 80 μL of sterile PBS and pretreated with 80 μL of poly-L-lysine for 15 min. A single-cell suspension of 5×10^5 GFP-transfected T24 cells in 100 μL of PBS was inoculated into the bladder and preserved for 1 h.

During the entire procedure, the mice remained under anesthesia for 2 h before the catheter was gently removed from the urethra. The mice were monitored every day for any signs of pain and distress. The nu/nu female mice bearing BCa were anesthetized by inhalation of 1%–2% isoflurane in an oxygen gas mixture and were placed on a heated platform during the catheterization procedures. Lubricated angiocatheters were inserted into the urethra. After full insertion, the bladder was flushed with 80 μL of sterile PBS. Either R11 (0.25 μM) or PBS was intravesically instilled and preserved for 1 h. After washing with PBS, 100 μL of NP5 nanocomplexes (with a concentration of Cy5-labeled DNA of 0.5 μM) was intravesically instilled and preserved for 2 h. The bladder was washed with PBS twice. The mice were sacrificed immediately. The tissues (including the bladder, heart, liver, spleen, lung and kidney) were harvested. The relative amount of DNA accumulated in the tissues was measured by using an in vivo imaging system (IVIS Lumina XRMS Series III (PerkinElmer), PerkinElmer Inc., Waltham, US) with an excitation wavelength of 640 nm and an emission wavelength of 660 nm. The tissues were frozen and sectioned (20 μm thick) in a cryostat. The sections were examined by using CLSM.

Statistical Analysis

Data are expressed as the means ± standard deviations (SD). Significant differences were determined using Student's *t* test or one-way ANOVA as appropriate. A 2-tailed $p<0.05$ was considered to be statistically significant. *$p<0.05$; **$p<0.01$; ***$p<0.001$; ****$p<0.0001$. All data were analyzed with GraphPad Prism Version 8.4.0.

Results and Discussion

Arginine-rich peptides are positively charged and can interact with the negatively charged phosphate backbone of DNA through electrostatic interactions. These peptides are known to enhance the condensation of DNA to small particles.[10] Herein, R11 was used for the condensation of a 30 nt single-strand DNA with a random sequence to construct nanocomplexes at a nitrogen-to-phosphate (NP) ratio of 5, 10 and 20. In this study, the condensation reaction of short-length ssDNA using arginine-rich peptides was utilized because of the newly emerging role of short-length ssDNA, including DNAzymes[14] and antisense oligonucleotides, as gene silencing therapeutics.[15] Figure 1A shows the size and zeta potential of free R11 or the nanocomplexes diluted in PBS buffer. Free R11 seemed to assemble into a microsized structure because R11 contained hydrophilic guanidino groups and hydrophobic 5-TAMRA molecules.[16] Increasing the amount of DNA that was incorporated into the nanocomplexes led to a decrease in the complex size. Nanocomplexes at an NP ratio of 5 presented the smallest diameter of 275.0 ±2.0 nm. The zeta potential of the nanocomplexes decreased with increasing amounts of doped DNA. Figure 1B presents the morphology of all types of nanocomplexes. By keeping the concentration of R11 constant, the diameter of the formed nanocomplexes decreased as more DNA was complexed with R11. The efficiency of condensation determined the morphology.[17] Interconnected linear structures were identified in the NP10 nanocomplexes and NP20 nanocomplexes. The NP5 nanocomplexes were determined to exhibit more compacted flower-like structures. Spherical micelles generated from free R11 could be observed. The condensation efficiency was tested by gel electrophoresis (Figure 1C). The amount of DNA stayed constant in this test. Free DNA migrated to the expected band, which was representative of DNA with a molecular weight less than 100 Kb. The gel retarding effect was obvious for the nanocomplexes at NP ratios of 10 and 20, rather than 5. Dissociation bands could be observed at NP ratios of 5 and 10. As indicated in Figure 1D and E, when the concentration of one component remained constant, increasing the probe concentration of the other component led to a decline in the

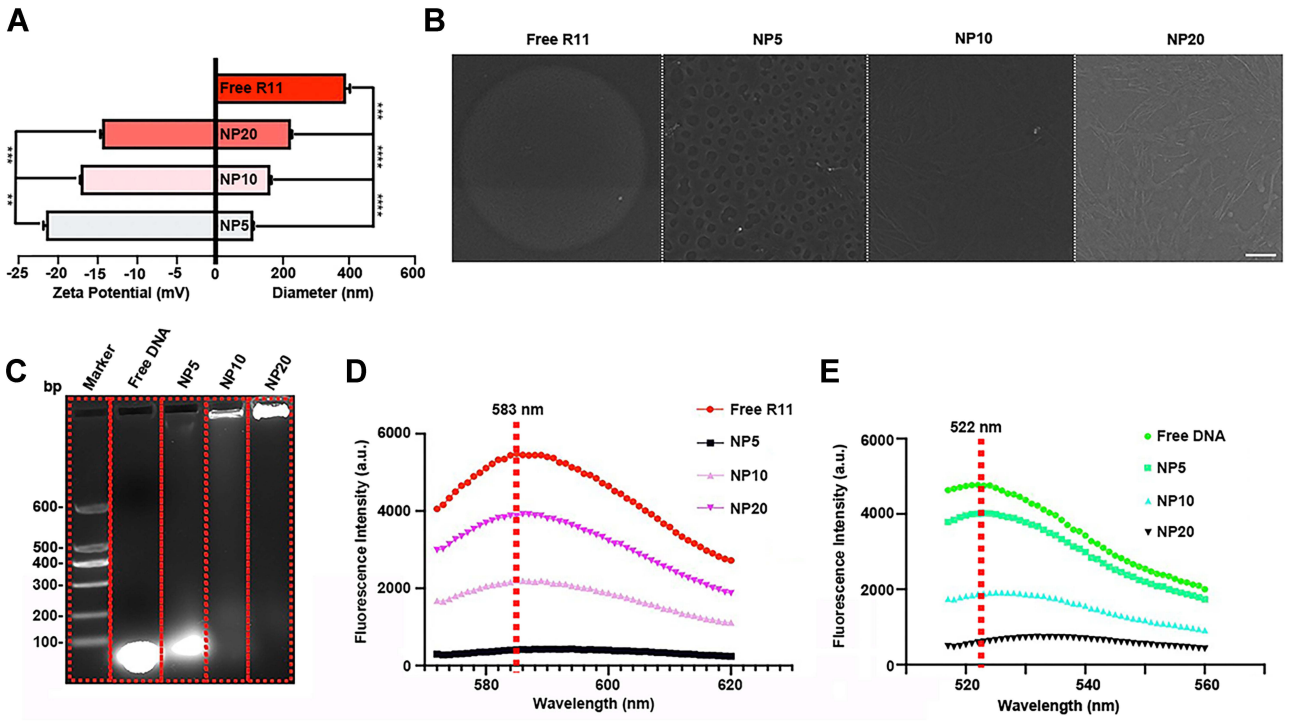

Figure 1 Physicochemical properties of nanocomplexes at different NP ratios.
Notes: Size distribution and zeta potential, **p < 0.01, ***p < 0.001, ****p < 0.0001 (**A**); scanning electron microscopy images of the nanocomplexes, scar bar: 100 μm (**B**); gel electrophoresis (**C**); fluorescence spectra of the R11 component of nanocomplexes at different NP ratios (**D**); fluorescence spectra of the DNA component of nanocomplexes at different NP ratios (**E**).
Abbreviations: NP, nitrogen-to-phosphate; R11, hendeca-arginine peptide.

intensity of the fluorescence signal, probably via self-quenching.[18] All evidence supported that R11 could condense DNA into nanosized structures. It is worth noting that a more compact size was achieved but the nanocomplex was less stable at an NP ratio of 5. Supplementary Figure 1 shows the nontoxicity of nanocomplexes with different R11 concentrations up to 4.0 μM.

R11 was previously proven to target BCa.[19] When DNA was polymerized with R11, the targeting efficiency of the nanocomplexes was expected to be enhanced. In this study, one normal urothelial cell line (SVHUC-1) and two BCa cell lines (T24 and 253J) were used. Figure 2A and C show that the specificity of the R11 component of the nanocomplexes for BCa was enhanced. The fluorescence intensity of T24 and 253J was determined to be approximately twice that of SVHUC-1 in the free R11 group. At an NP ratio of 5, the fluorescence intensity of T24 and 253J was determined to be 6.5±0.3 and 4.2±0.0 times, respectively, that of SVHUC-1. The specificity of the DNA component of the nanocomplexes for BCa is shown in Figure 2B and D. The fluorescence intensity of T24 and 253J was calculated to be 4.6±0.0 and 3.6±0.1 times that of SVHUC-1 at an NP ratio of 5. The nanocomplexes (NP ratio=5) for BCa exhibited the best specificity; thus, the nanocomplexes are worth further examining for applications in delivering nucleic acid into BCa.

Noncovalent interactions are usually labile and weak.[20] The negatively charged permeation barrier might competitively interact with the R11 component[4] and disrupt the stability of the nanocomplexes. Herein, free R11 was used to block the interaction between the permeation barrier and the R11 component of the nanocomplexes. The GAG layer is the first permeation barrier and is mainly composed of chondroitin sulfate.[21] Figure 3 indicates that the permeation rate of the DNA component through the GAG layer ranged from 32.0±0.9% to 59.1±0.2%, while the condition of R11 pretreatment promoted the permeation rate to the range from 56.3±1.3% to 100±0.2%. Another issue to consider was the integrity of the nanocomplexes when they contacted the negatively charged plasma membrane, which serves as the second permeation barrier during the whole process of DNA delivery. Within the first 80 min, the correlation of R11 and DNA colocalization was poor. At 100 min, a strong correlation of colocalization was observed in punctation areas at the membrane (Figure 4A). The dynamic change in the spatial relationship between the R11 component and the DNA component indicated that the nanocomplexes dissociated at the early phase of

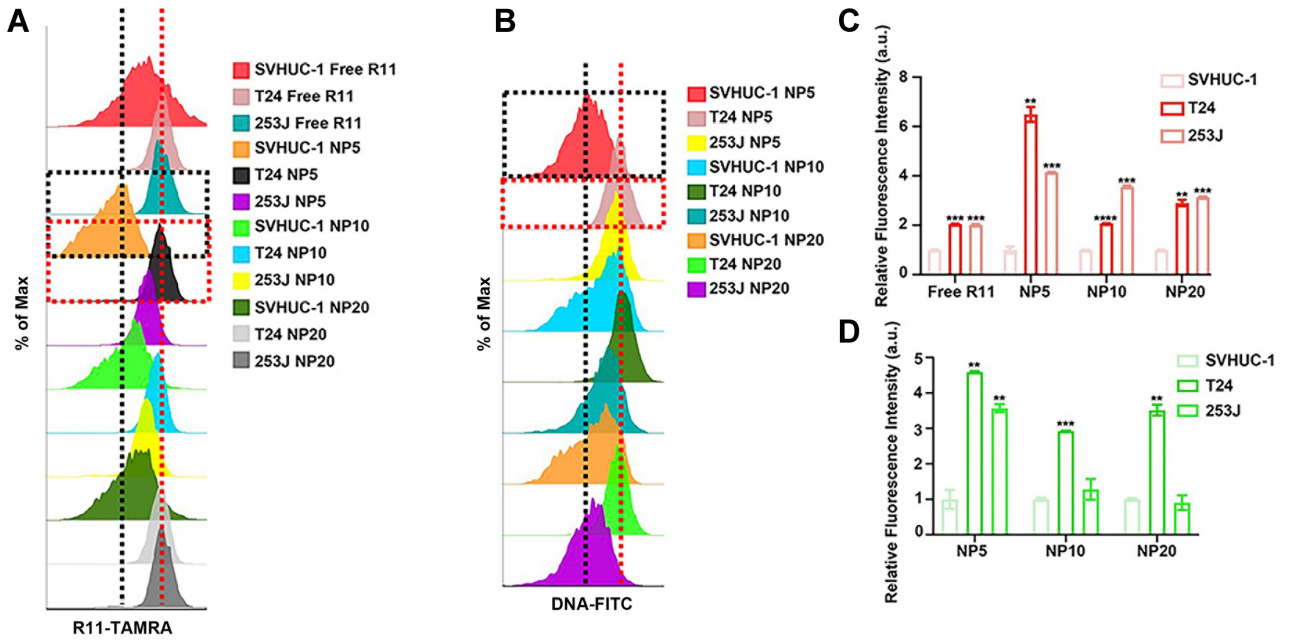

Figure 2 BCa targeting efficiency of nanocomplexes at different NP ratios.
Notes: Flow cytometry analysis of BCa targeting efficiency of the R11 component, the black dotted line shows the peak of SVHUC-1 treated with NP5, the red dotted line shows the peak of T24 treated with NP5 (**A**); Flow cytometry analysis of BCa targeting efficiency of DNA component, the black dotted line shows the peak of SVHUC-1 treated with NP5, the red dotted line shows the peak of T24 treated with NP5 (**B**); Relative fluorescence intensity of the R11 component in different cell lines, significance analysis: SVHUC-1 and BCa cell lines inside the same subgroup, $^{**}p < 0.01$, $^{***}p < 0.001$ (**C**); Relative fluorescence intensity of DNA component in different cell lines, significance analysis: SVHUC-1 and BCa cell lines inside the same subgroup, $^{**}p < 0.01$, $^{***}p < 0.001$ (**D**).
Abbreviations: BCa, bladder cancer; NP, nitrogen-to-phosphate; R11, hendeca-arginine peptide.

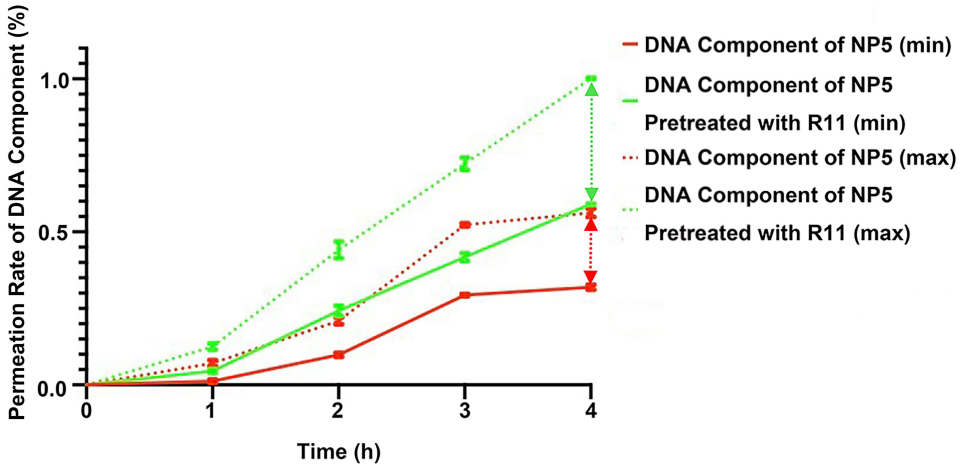

Figure 3 The GAG permeation assay of the DNA component.
Notes: The green double-headed arrow and red double-headed arrow show the range of the permeation rate with or without R11 pretreatment (0.25 μM), respectively.
Abbreviation: GAG, glycosaminoglycan.

transmembrane delivery and reassembled afterward. A strong correlation of colocalization occurred earlier (at 60 min) with R11 pretreatment (Figure 4B). With the R11 pretreatment (at a concentration of 0.25 μM), a maximum amount of internalized DNA was reached in T24 cells. The specificity was quantified to be 1.5±0.0-fold higher than that in the group pretreated with 0 μM R11 (Figure 5A and B). When R11 (0.25 μM) and the nanocomplexes were applied at the same time, the specificity increased only by 1.1±0.0-fold when compared with that in the group pretreated with 0 μM R11 (Figure 5B). We proved that R11 pretreatment, rather than coincubation, preserved the stability of nanocomplexes to some extent and improved the delivery efficiency and BCa-

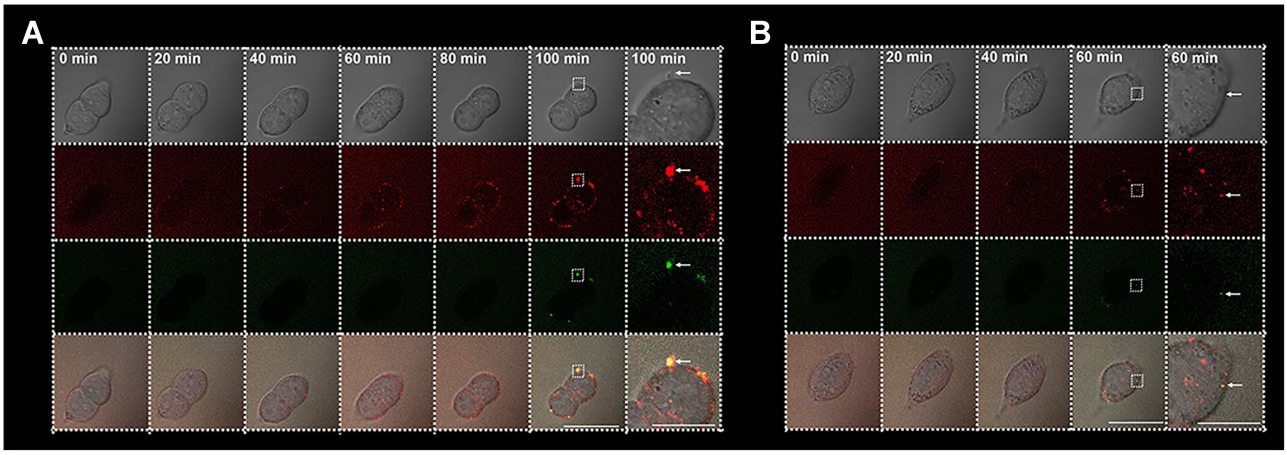

Figure 4 The colocalization of the R11 component (red) and the DNA (green) component at the plasma membrane.
Notes: After 0 μM R11 pretreatment (with the arrow showing the re-polymerized assembly), Scar bar: 25 μm (**A**); After 0.25 μM R11 pretreatment (with the arrow showing the repolymerized assembly), Scar bar: 25 μm (**B**).
Abbreviation: R11, hendeca-arginine peptide.

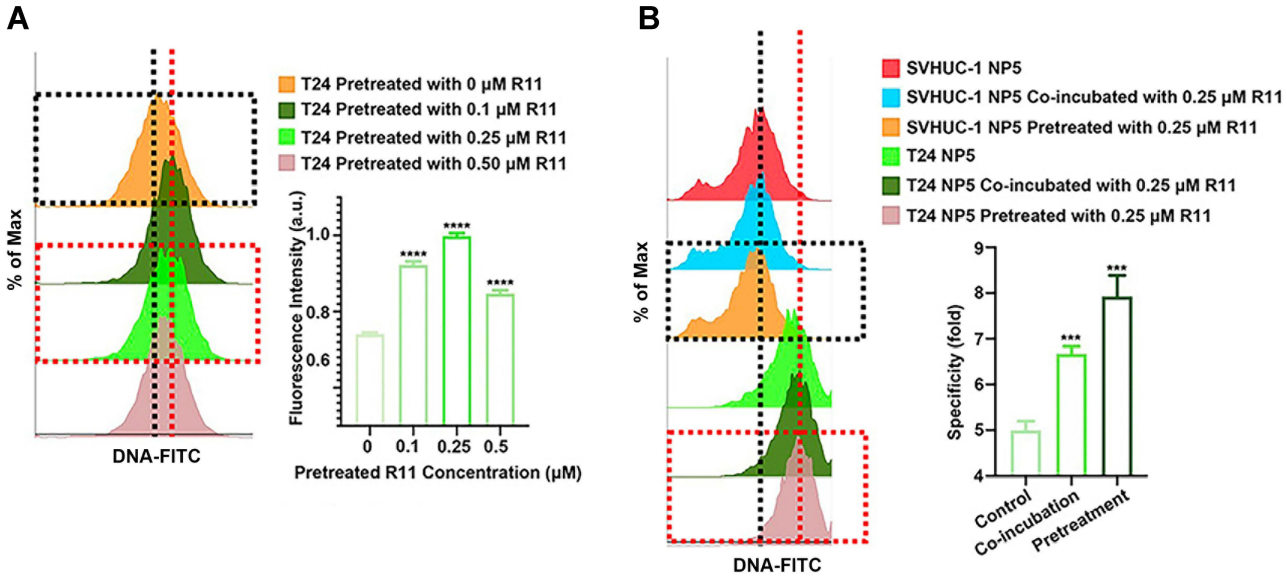

Figure 5 The internalized amount of the DNA component on different conditions.
Notes: Flow cytometry analysis of the increase in the internalized amount of the DNA component after T24 cells were pretreated with R11 of different concentrations, the black dotted line shows the peak of T24 pretreated with 0 μM R11, the red dotted line shows the peak of T24 pretreated with 0.25 μM R11, significance analysis: T24 pretreated with 0 μM R11 and T24 pretreated with R11 of other different concentrations, ****$p < 0.0001$ (**A**); Flow cytometry analysis of the increase in the internalized amount of the DNA component after T24 cells were pretreated with 0.25 μM R11 or co-incubated with 0.25 μM R11, the black dotted line shows the peak of SVHUC-1 pretreated with 0.25 μM R11, the red dotted line shows the peak of T24 pretreated with 0.25 μM R11, significance analysis: Control and T24 pretreated with 0.25 μM R11 or T24 co-incubated with 0.25 μM R11, ***$p < 0.001$ (**B**).
Abbreviation: R11, hendeca-arginine peptide.

targeting efficiency of DNA across the plasma membrane. Next, the mechanism of cellular uptake was studied. Low temperature (4 °C) completely inhibited the cellular uptake of the nanocomplexes, indicating that an energy-dependent endocytosis pathway was involved. Macropinocytosis represented the main endocytosis pathway for both components regardless if R11 pretreatment was applied (Figure 6). R11 pretreatment nearly eliminated the clathrin-mediated endocytosis (CME) pathway for both components while increasing the internalized amount of the DNA component through clathrin-independent endocytosis (CIE) (Figure 6C and D). The spatial correlation of the two components was strong for endocytic nanocomplexes in the absence of R11 pretreatment (Figure 7A). R11 pretreatment allowed the DNA component to cover more areas of the cytoplasm than that of the

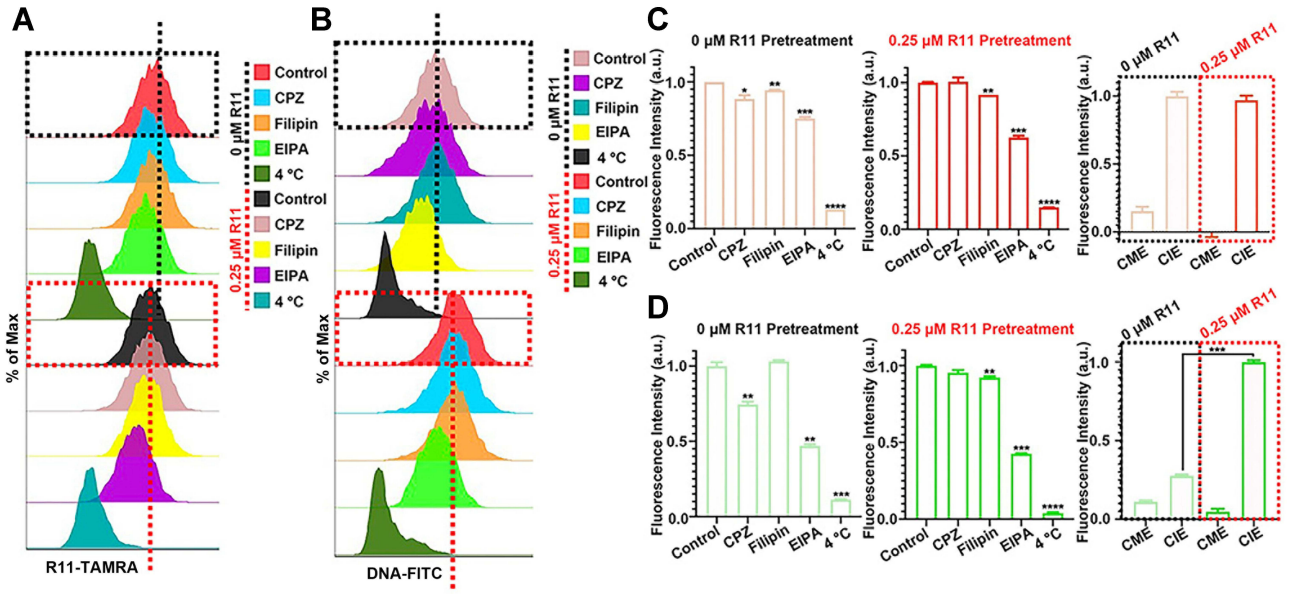

Figure 6 Endocytosis inhibition of nanocomplexes.

Notes: Flow cytometry analysis of endocytosis inhibition of R11 component, black dotted line: peak of control pretreated with 0 μM R11, Red dotted line: peak of control pretreated with 0.25 μM R11 (**A**); Endocytosis inhibition of DNA component, black dotted line: peak of control pretreated with 0 μM R11, red dotted line: peak of control pretreated with 0.25 μM R11 (**B**); Statistic analysis of endocytosis inhibition of R11 component, significance analysis: control and T24 treated with different endocytosis inhibitors, significance analysis: R11 component endocytosed through CIE in T24 pretreated with 0 μM R11 and R11 component endocytosed through CIE in T24 pretreated with 0.25 μM R11, *p < 0.05, **p < 0.01, ***p < 0.001, ****p < 0.0001 (**C**); Statistic analysis of endocytosis inhibition of DNA component, significance analysis: control and T24 treated with different endocytosis inhibitors, significance analysis: DNA component endocytosed through CIE in T24 pretreated with 0 μM R11 and DNA component endocytosed through CIE in T24 pretreated with 0.25 μM R11, **p < 0.01, ***p < 0.001, ****p < 0.0001 (**D**).

Abbreviations: R11, hendeca-arginine peptide; CME, clathrin-mediated endocytosis; CIE, clathrin-independent endocytosis; CPZ, chlorpromazine hydrochloride; EIPA, ethylisopropylamiloride.

R11 component (Figure 7B). The nonlysosome-localized proportion of internalized DNA determines the efficiency by which the DNA can directly contact its target sequence.[22] Without R11 pretreatment, the DNA component was mostly confined to LysoTracker-stained lysosomes, but the nonlysosome-localized proportion of the DNA component increased upon R11 pretreatment (Figure 7C and D). Furthermore, R11 pretreatment corrected the intracellular trafficking of the DNA component toward the nucleus (Figure 7E and F).

The third permeation barrier is composed of densely packed BCa cell aggregates and a dense extracellular matrix.[5,23,24] The method by which intravesically administered drugs reach distant BCa cells solely depends on the direct penetration of drugs across the third permeation barrier in a layer-by-layer manner.[3] Multicellular spheroids (MCSs) have been proposed as an in vitro 3D-cultured tumor model to evaluate the tumor penetration of drugs.[13] T24 MCSs were established to study the penetration efficiency. As shown in Figure 8A–C, either free R11 or the R11 component in the nanocomplexes could penetrate deep into MCSs with similar efficiency. EXO1, an exocytosis inhibitor,[13] and the endocytosis inhibitor cocktail (which is composed of CPZ, filipin and EIPA) could not prevent their penetration. However, the EXO1 and endocytosis inhibitor cocktail could prevent the penetration of the DNA component in the nanocomplexes (Figure 8D–F), and the DNA component showed retarded migration in MCSs compared with that of the R11 component (Figure 8G and H). The R11 component used to repolymerize the DNA component was depleted after several rounds of infiltration, which might contribute to the variance of the penetration behavior shown by the two components. R11 pretreatment allowed the DNA component to penetrate deeper into the MCSs (Figure 8G–I), further proving that R11 pretreatment might improve the stability of nanocomplexes against the electrostatic interaction between the third permeation barrier and the R11 component.

The penetration of free R11 and the two components in the nanocomplexes could be attributed to two possible mechanisms. One is paracellular diffusion through the extracellular matrix,[25] and the other is transcellular transport.[26] For the first mechanism, the Transwell membrane was coated with Matrigel to mimic the extracellular matrix.[27] A total of 18.3±0.6% of free R11 could pass through the Matrigel, in which nearly all DNA leaked to the lower chamber. For the

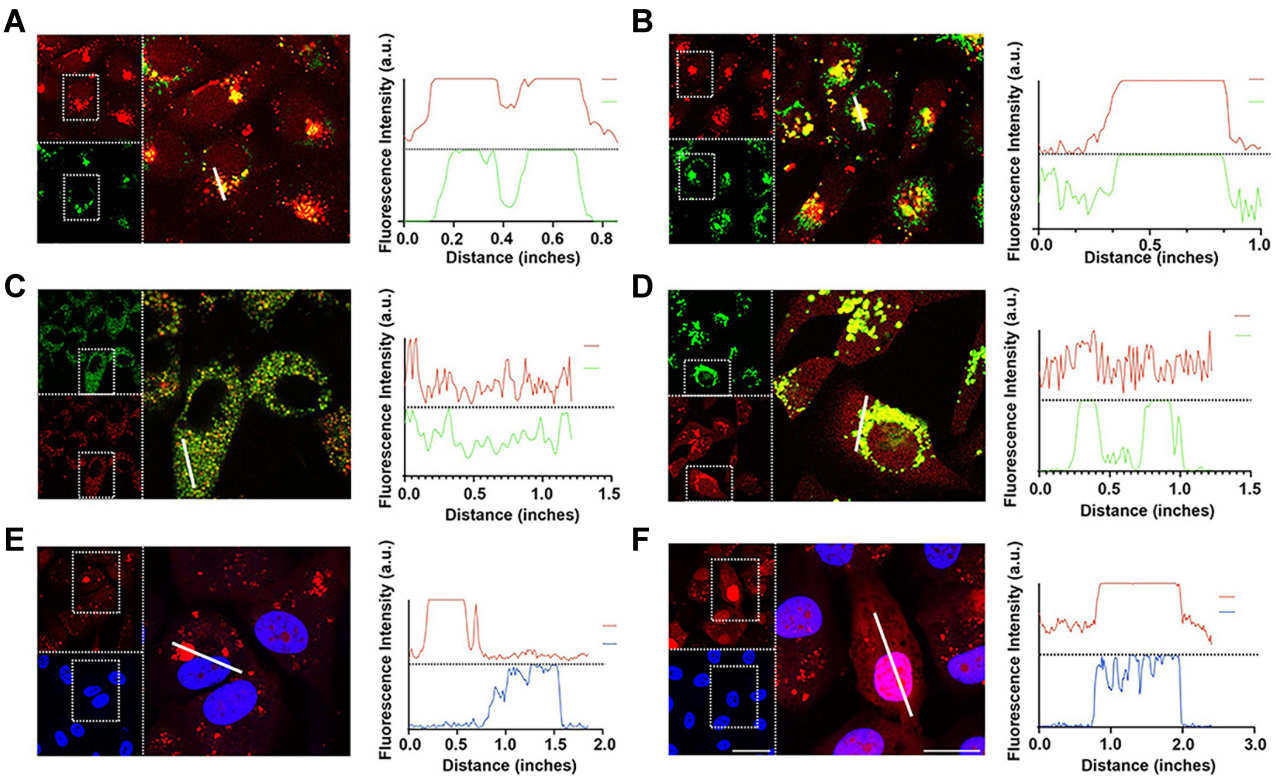

Figure 7 Subcellular distribution of the DNA component.
Notes: Colocalization of the DNA component (green) and the R11 component (red) after 0 μM R11 pretreatment, the dotted line shows the fluorescence baseline, scar bar: 25 μm (**A**); Colocalization of the DNA component (green) and the R11 (red) component after 0.25 μM R11 pretreatment, the dotted line shows the fluorescence baseline, scar bar: 25 μm (**B**); Colocalization of the DNA component (red) and the lysosome (green) after 0 μM R11 pretreatment, the dotted line shows the fluorescence baseline, scar bar: 25 μm (**C**); Colocalization of the DNA component (red) and the lysosome (green) after 0.25 μM R11 pretreatment, the dotted line shows the fluorescence baseline, scar bar: 25 μm (**D**); Colocalization of the DNA component (red) and the nucleus (blue) after 0 μM R11 pretreatment, the dotted line shows the fluorescence baseline, scar bar: 25 μm (**E**); Colocalization of the DNA component (red) and the nucleus (blue) after 0.25 μM R11 pretreatment, the dotted line shows the fluorescence baseline, Scar bar: 25 μm (**F**).
Abbreviation: R11, hendeca-arginine peptide.

nanocomplexes, the permeation rate of the R11 component ranged from 19.4±0.5% to 100%, while that of the DNA component was 100% (Figure 9A). The mechanism of paracellular diffusion through the extracellular matrix was inconsistent with that observed in T24 MCSs. Hence, transcellular transport played a major role in the penetration behavior of free R11 and the two components. All of the above cargos were confined to first-generation cells that received free R11- or nanocomplex-containing medium. Cargoes could not be transported to the second-generation or third-generation cells that received medium that contained only compounds secreted by the first-generation or second-generation cells (Figure 9B). Therefore, transcytosis was not the mechanism of transcellular transport.[5] Direct intercellular contact is necessary for the direct transfer of cargos, which was shown to be highly efficient in the intercellular exchange of cargos.[28,29] As suggested in Figure 9C, the percentage of the positively stained cell population through direct transfer was 31.0±2.5%, 25.1±0.7%, 51.5±3.7% and 93.8±1.4% for free R11, the R11 component, the DNA component and the DNA component combined with R11 pretreatment, respectively. As suggested in Figure 9D, the transferred fluorescence intensity relative to that of the first-generation cells was 55.0±3.4%, 44.0±1.1%, 24.6±0.4%, 53.7±11.6% for free R11, the R11 component, the DNA component and the DNA component combined with R11 pretreatment, respectively. These results proved that free R11 and nanocomplexes were transported through direct transfer, in which the stepwise method boosted the intercellular trafficking of the DNA component.

The positive role of the stepwise method in increasing the targeting capacity and penetration efficiency of the DNA component was confirmed in murine orthotropic BCa models. After a single instillation, R11 pretreatment led to a 9.4 ±4.8-fold increase in the fluorescence of the DNA component accumulated in the bladder, and none of the DNA leaked to organs, such as the heart, liver, spleen, lung and kidney (Figure 10A and B). Under a microscope, the DNA component

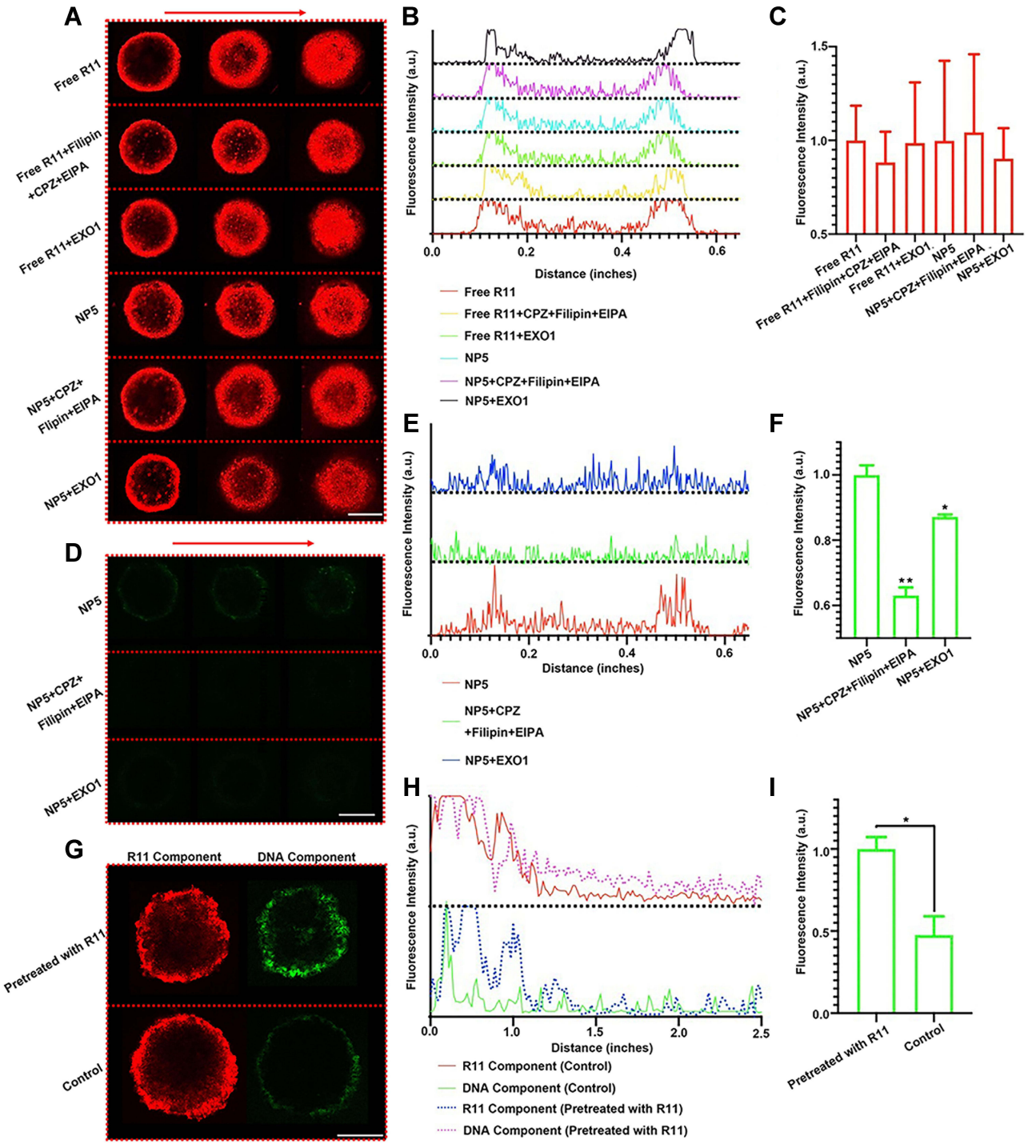

Figure 8 Penetration of nanocomplexes into tumor spheroids.

Notes: CLSM analysis of R11 penetration in tumor spheroids, the red arrow shows the direction from the intermediate layer to the upper layer, scar bar: 200 μm (**A**); Fluorescence distribution of R11 along the diameter of tumor spheroids, the dotted line shows the fluorescence baseline (**B**); Statistical analysis of fluorescence of R11-stained tumor spheroids, significance analysis: free R11 and free R11+different inhibitors, significance analysis: R11 component and R11 component + different inhibitors (**C**); CLSM analysis of DNA penetration in tumor spheroids, the red arrow shows the direction from the intermediate layer to the upper layer, scar bar: 200 μm (**D**); Fluorescence distribution of DNA along the diameter of tumor spheroids, the dotted line shows the fluorescence baseline (**E**); Statistical analysis of fluorescence of DNA-stained tumor spheroids, significance analysis: DNA component and DNA component + different inhibitors (**F**); CLSM analysis of R11 (red) and DNA (green) in tumor spheroids, scar bar: 200 μm, **$p < 0.01$, ***$p < 0.001$ (**G**); Colocalization of DNA and R11 in tumor spheroids along the diameter of tumor spheroids, the dotted line shows the fluorescence baseline (**H**); Statistical analysis of the amount of DNA in tumor spheroids, significance analysis: control and T24 pretreated with 0.25 μM R11, *$p < 0.05$ (**I**).

Abbreviations: R11, hendeca-arginine peptide; CPZ, chlorpromazine hydrochloride; EIPA, ethylisopropylamiloride; CLSM, confocal laser scanning microscopy.

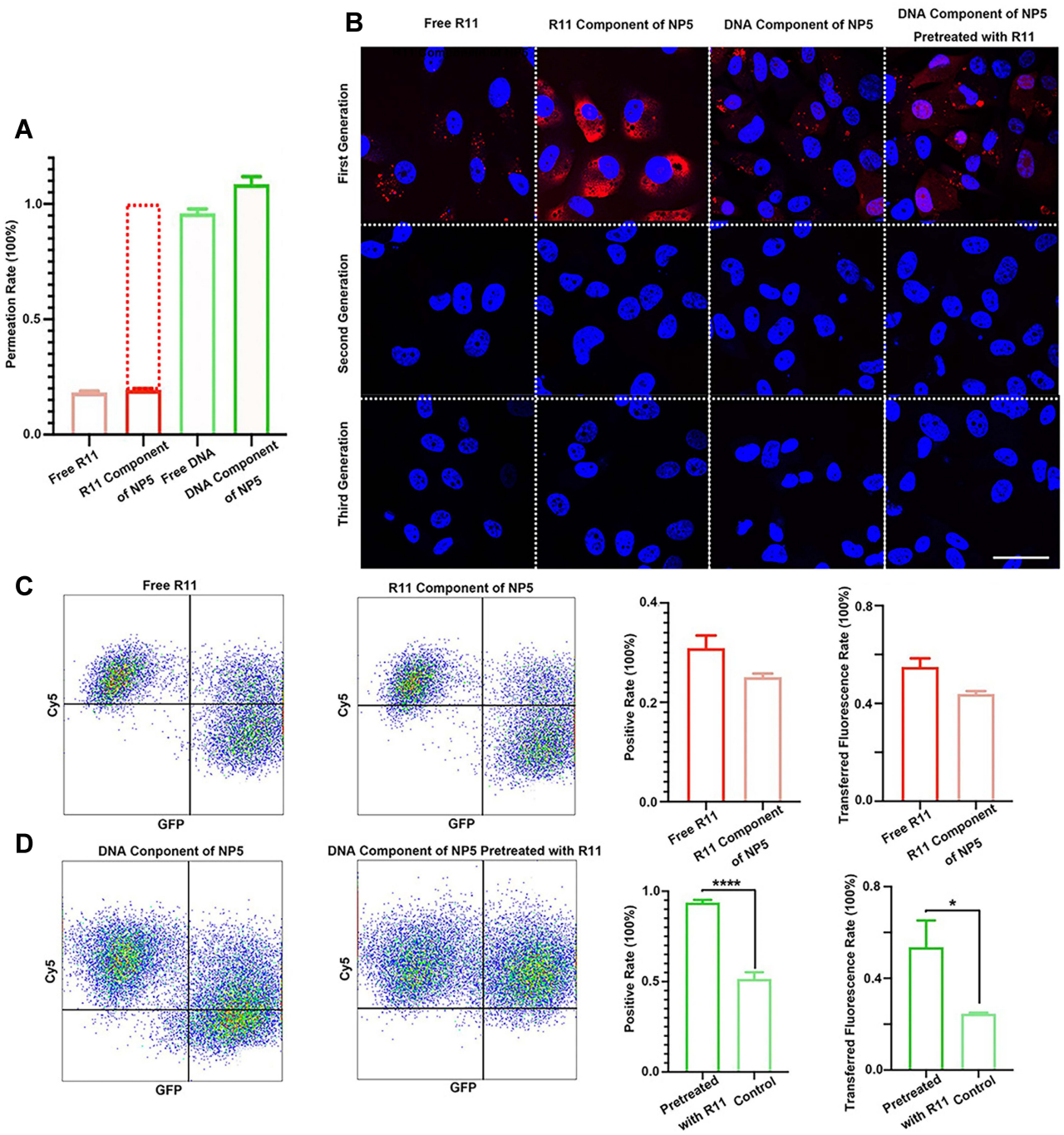

Figure 9 Determination of the penetration mechanism.
Notes: The Matrigel permeation assay (**A**); The transcytosis assay of cells after different treatments, scar bar: 25 μm (**B**); Flow cytometry analysis and statistical analysis of direct transfer efficiency of R11 (**C**); Flow cytometry analysis and statistical analysis of the direct transfer efficiency of DNA, significance analysis: positive rate or transferred fluorescence rate of the control and T24 pretreated with 0.25 μM of R11, *p < 0.05, ****p < 0.0001 (**D**).
Abbreviations: R11, hendeca-arginine peptide; GAG, glycosaminoglycan.

was found to barely adhere to the BCa, but R11 pretreatment enabled the DNA component to specifically accumulate in BCa, as reflected by the fact that Cy5 fluorescence is found exactly in GFP-labeled tumor areas (Figure 10C and D). R11 pretreatment increased the intensity of Cy5 fluorescence of tumor areas by 16.0±5.5-fold (Figure 10E). The fluorescence signal did not fade even in the inner space of tumors (Figure 10F). HE staining indicated that nanocomplexes caused no toxicity to normal organs regardless of whether R11 pretreatment was applied (Figure 10G).

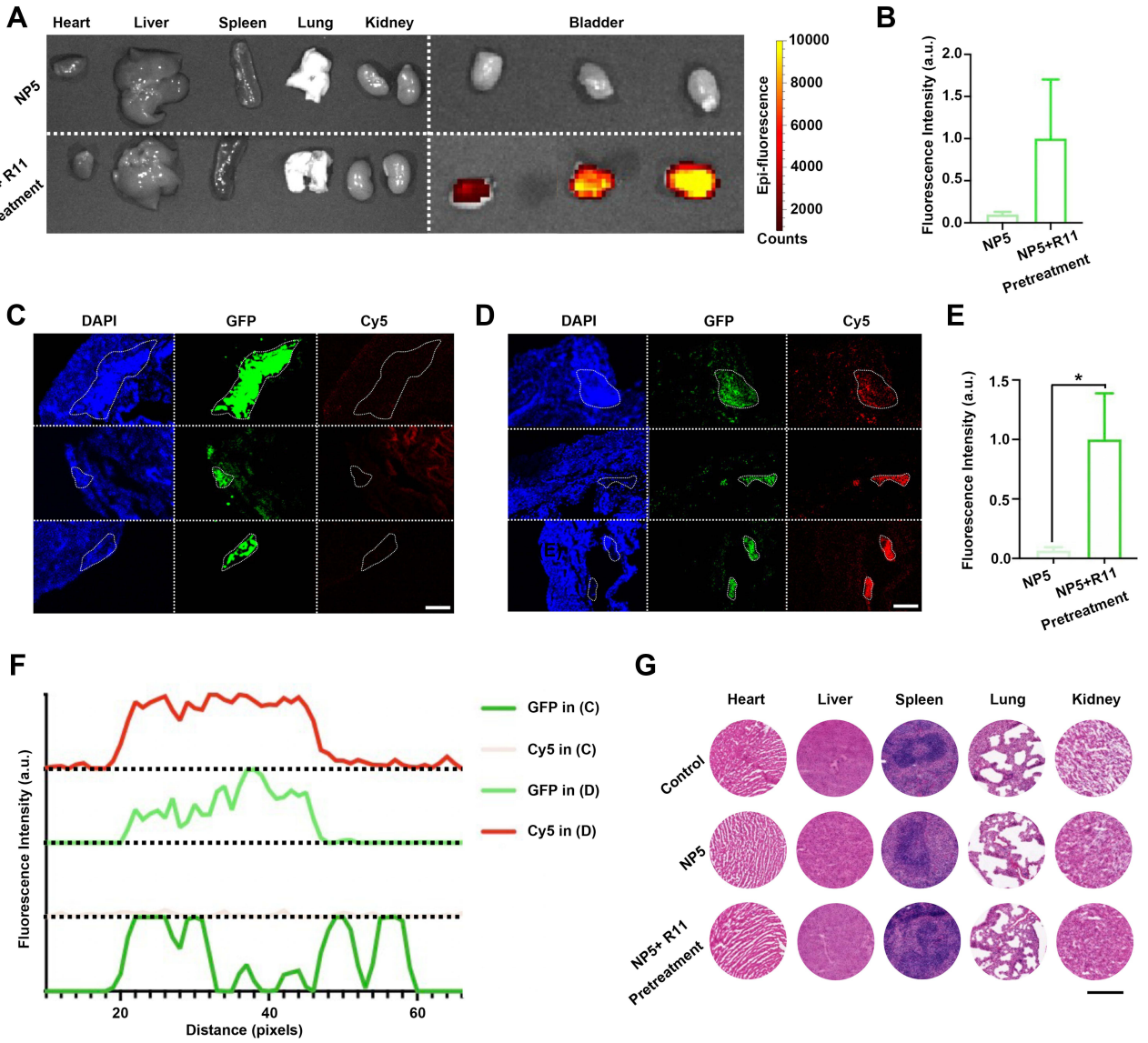

Figure 10 Intravesical instillation of nanocomplexes in murine orthotopic BCa models.
Notes: The amount of DNA accumulated in bladder tissues as illustrated by GFP fluorescence (**A**); Statistical analysis of the amount of DNA accumulated in bladder tissues, significance analysis: NP5 nanocomplexes and NP5 nanocomplexes + 0.25 μM R11 pretreatment (**B**); The colocalization of DNA (Cy5) and the tumor area (GFP) after 0 μM R11 pretreatment was applied, scar bar: 100 μm (**C**); The colocalization of DNA (Cy5) and the tumor area (GFP) after 0.25 μM R11 pretreatment was applied, scar bar: 100 μm (**D**); Statistical analysis of the amount of DNA accumulated in bladder tumors, significance analysis: NP5 nanocomplexes and NP5 nanocomplexes + 0.25 μM R11 pretreatment, *$p < 0.05$ (**E**); Fluorescence distribution of DNA (Cy5) along the diameter of tumor tissues (GFP), the dotted line represents fluorescence baseline, scar bar: 100 μm (**F**); HE staining of the organs in mice in different treatment groups, scar bar: 500 μm (**G**).
Abbreviations: BCa, bladder cancer; R11, hendeca-arginine peptide.

Conclusion

In this study, we utilized R11 and R11-DNA nanocomplexes in a stepwise manner as gene delivery platforms to enhance the targeting and penetration efficiency of IT. In particular, the stepwise method improved the cellular uptake efficiency of the DNA component, corrected their intracellular trafficking, and boosted intercellular transport through the mechanism of direct transfer. As a result, R11 pretreatment allowed the DNA component to target and penetrate BCa with high efficiency in vivo. Our stepwise method combined with R11-DNA nanocomplexes shows promising potential for further clinical use, but compared to the standard intravesical therapy protocol, it was slightly more time-consuming. Considering the tolerance to intravesical therapy, the stepwise method should be further modified to meet clinical demands.

Acknowledgments

This research was funded by Medical Technology Plan of Zhejiang Province (grant number: 2021421701), Medical Technology Plan of Zhejiang Province (grant number: 2022497314), the Natural Science Foundation of Zhejiang Province (grant number: LQ21H160041), the Natural Science Foundation of Zhejiang Province (grant number: LY18H160040), the Health Commission of Zhejiang Province's Young Talents Project (grant number: 2018RC001).

Disclosure

The authors report no conflicts of interest in this work.

References

1. Bray F, Ferlay J, Soerjomataram I., et al. Global cancer statistics 2018: GLOBOCAN estimates of incidence and mortality worldwide for 36 cancers in 185 countries. *CA Cancer J Clin*. 2018;68:394–424.
2. Lenis AT, Lec PM, Chamie K. Bladder cancer a review. *JAMA*. 2020;324:1980–1991.
3. Joice GA, Bivalacqua TJ, Kates M. Optimizing pharmacokinetics of intravesical chemotherapy for bladder cancer. *Nat Rev Urol*. 2019;16:599–612.
4. Serrano Cardona L, Muñoz Mata E. Recent Advances in Intravesical Drug/Gene Delivery. *Early Hum Dev*. 2013;83:1–11.
5. Chen S, Zhong Y, Fan W, et al. Enhanced tumour penetration and prolonged circulation in blood of polyzwitterion–drug conjugates with cell-membrane affinity. *Nat Biomed Eng*. 2021;5:1019–1037.
6. Sun L, Wang D, Chen Y, et al. Core-shell hierarchical mesostructured silica nanoparticles for gene/chemo-synergetic stepwise therapy of multidrug-resistant cancer. *Biomaterials*. 2017;133:219–228.
7. Manju S, Sreenivasan K. Gold nanoparticles generated and stabilized by water soluble curcumin-polymer conjugate: blood compatibility evaluation and targeted drug delivery onto cancer cells. *J Colloid Interface Sci*. 2012;368:144–151.
8. Zacchè MM, Srikrishna S, Cardozo L. Novel targeted bladder drug-delivery systems: a review. *Res Reports Urol*. 2015;7:169–178.
9. Ma M, Zhang P, Liang X, et al. R11 peptides can promote the molecular imaging of spherical nucleic acids for bladder cancer margin identification. *Nano Res*. 2021;15:2278–2287.
10. Saccardo P, Villaverde A, González-Montalbán N. Peptide-mediated DNA condensation for non-viral gene therapy. *Biotechnol Adv*. 2009;27:432–438.
11. Mann A, Richa R, Ganguli M. DNA condensation by poly-l-lysine at the single molecule level: role of DNA concentration and polymer length. *J Control Release*. 2008;125:252–262.
12. Dai J, Cheng Y, Wu J, et al. Modular peptide probe for pre/intra/postoperative therapeutic to reduce recurrence in ovarian cancer. *ACS Nano*. 2020;14:14698–14714.
13. Zhou Q, Shao S, Wang J, et al. Enzyme-activatable polymer–drug conjugate augments tumour penetration and treatment efficacy. *Nat Nanotechnol*. 2019;14:799–809.
14. Meng L, Ma W, Lin S, et al. Tetrahedral DNA nanostructure-delivered DNAzyme for gene silencing to suppress cell growth. *ACS Appl Mater Interfaces*. 2019;11:6850–6857.
15. Le BT, Raguraman P, Kosbar TR, et al. Antisense oligonucleotides targeting angiogenic factors as potential cancer therapeutics. *Mol Ther Nucleic Acids*. 2019;14:142–157.
16. Futaki S, Nakase I. Cell-surface interactions on arginine-rich cell-penetrating peptides allow for multiplex modes of internalization. *Acc Chem Res*. 2017;50:2449–2456.
17. Mann A, Thakur G, Shukla V, et al. Differences in DNA condensation and release by lysine and arginine homopeptides govern their DNA delivery efficiencies. *Mol Pharm*. 2011;8:1729–1741.
18. Gracie K, Smith WE, Yip P, et al. Interaction of fluorescent dyes with DNA and spermine using fluorescence spectroscopy. *Analyst*. 2014;139:3735–3743.
19. Du Y, Wang L, Wang W, et al. Novel Application of Cell Penetrating R11 Peptide for Diagnosis of Bladder Cancer. *J Biomed Nanotechnol*. 2018;14:161–167.
20. Ulrich S. Growing prospects of dynamic covalent chemistry in delivery applications. *Acc Chem Res*. 2019;52:510–519.
21. Janssen DAW, Van Wijk XMR, Jansen KCFJ, et al. The distribution and function of chondroitin sulfate and other sulfated glycosaminoglycans in the human bladder and their contribution to the protective bladder barrier. *J Urol*. 2013;189:336–342.
22. Rathore B, Sunwoo K, Jangili P, et al. Nanomaterial designing strategies related to cell lysosome and their biomedical applications: a review. *Biomaterials*. 2019;211:25–47.
23. Gu L, Duan Z, Chen X, et al. A transformable amphiphilic and block polymer−dendron conjugate for enhanced tumor penetration and retention with cellular homeostasis perturbation via membrane flow. *Adv Mater*. 2022;34:2200048.
24. Luo Q, Duan Z, Li X, et al. Branched Polymer-Based Redox/Enzyme-Activatable Photodynamic Nanoagent to Trigger STING-Dependent Immune Responses for Enhanced Therapeutic Effect. *Adv Funct Mater*. 2022;32:2110408.
25. Bugno J, Hsu HJ, Pearson RM, et al. Size and surface charge of engineered poly(amidoamine) dendrimers modulate tumor accumulation and penetration: a model study using multicellular tumor spheroids. *Mol Pharm*. 2016;13:2155–2163.
26. Komin A, Bogorad MI, Lin R, et al. A peptide for transcellular cargo delivery: structure-function relationship and mechanism of action. *J Control Release*. 2020;324:633–643.
27. Khavari ND. Non-specific binding and steric hindrance thresholds for penetration of particulate drug carriers within tumor tissue. *Physiol Behav*. 2017;176:139–148.
28. Epperla CP, Mohan N, Chang CW, et al. Nanodiamond-Mediated Intercellular Transport of Proteins through Membrane Tunneling Nanotubes. *Small*. 2015;11:6097–6105.
29. Guo L, Zhang Y, Yang Z, et al. Tunneling nanotubular expressways for ultrafast and accurate m1 macrophage delivery of anticancer drugs to metastatic ovarian carcinoma. *ACS Nano*. 2019;13:1078–1096.